ELSEVIER

Journal of Photochemistry and Photobiology A: Chemistry 99 (1996) 155–163

Journal of PHOTOCHEMISTRY AND PHOTOBIOLOGY A:CHEMISTRY

Dynamics of aggregate formation and translational diffusion of a spiropyran studied by the transient grating method

Toshiya Okazaki, Noboru Hirota, Masahide Terazima *

Department of Chemistry, Graduate School of Science, Kyoto University, Kyoto 606, Japan

Received 17 April 1996; accepted 9 May 1996

Abstract

The molecular dynamics after the photoexcitation of 1',3',3'-trimethylspiro-8-nitro(2H-1-benzopyran-2',2'-indoline) (8-nitroBIPS) were investigated by the transient grating (TG) method. When the excitation laser power is low, the TG signal consists of three components which reflect the thermal diffusivity in the solution and the translational diffusion of the colourless and coloured forms of 8-nitroBIPS. The diffusion constant of the colourless form is found to be approximately 1.5 times larger than that of the coloured form, and this result is explained in terms of the photoinduced electric dipole moment of the coloured form. With stronger excitation light, another new TG signal is observed in the longer time region in non-polar solvents. This signal is attributed to the intensity grating produced by probe light scattering due to the microcrystals of 8-nitroBIPS. From the temporal profile of this new TG signal (aggregate grating signal), the dynamics of the aggregate formation process can be investigated.

Keywords: Aggregate formation; Spiropyran; Transient grating method; Translational diffusion

1. Introduction

Spiropyrans are prototypes of photochromic molecules, which have attracted the interest of scientists for a long time from various points of view [1]. On UV photoexcitation of a spiropyran in its colourless form (A), it is converted to a coloured merocyanine form (B). The merocyanine form is usually converted back to the original form thermally. However, if the spiropyran contains a nitro group and the photochromism occurs in non-polar solvents, another process, photoinduced aggregation, is sometimes observed. Compared with the extensive research carried out on the photochromic process, studies on aggregation, in particular the kinetic aspects of aggregate formation, have been very limited. In this study, we use the transient grating (TG) method to reveal the molecular dynamics after photoexcitation of 1',3',3'-trimethylspiro-8-nitro(2H-1-benzopyran-2',2'-indoline) (8-nitroBIPS) in polar and non-polar solvents: translational diffusion and aggregation.

Krongauz and coworkers [2–8] investigated the quasi-crystal formation on UV irradiation of 6-nitroBIPS in non-polar solvents. They found that dimers AB and complexes A_nB ($n=2, 3$) are combined to form microcrystals. These microcrystals wear amorphous envelopes which have smaller dipole moments than the microcrystals producing globules. The globules have very large permanent electric dipole moments. If a static electric field is applied to the solution, the globules form a string of bead structures (quasi-crystals) on a macroscopic scale due to the electric interaction between the field and the dipoles. Sato and coworkers [9–11] produced much larger aggregates by prolonged irradiation and discussed their molecular structures in terms of resonance Raman spectra. They also measured the temporal profiles of the absorption spectra at the merocyanine monomeric band and observed anomalous non-exponential decay behaviour, which was interpreted in terms of the deaggregation process of small aggregates. Kalisky and Williams [12,13] studied the transient absorption spectra of substituted 6-nitroBIPS. They observed a slow progressive red shift in the 640–670 nm region on photoirradiation and attributed the shift to the formation of J-aggregate-like stacks consisting of AB or A_nB ($n=2, 3$).

In this paper, we aim to clarify the formation process of small aggregates (microcrystals) by the time-resolved TG method. First, we investigate the translational diffusion of the A and B forms in ethanol and cyclohexane (Scheme 1). When the excitation light is sufficiently weak, the observed TG signal consists of three exponential decays. One is attributed to the thermal grating signal produced by the heat releas-

* Corresponding author.

PII S1010-6030(96)04404-8

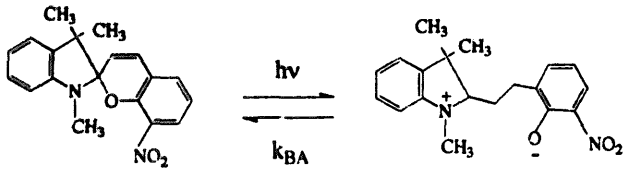

A B

Scheme 1.

ing process and the other two to the diffusion processes of the A and B forms in the solution (the species grating signal). From the former and latter components, the thermal diffusivity and the translational diffusion constants (D) of the A and B forms respectively are determined. D of the A form is found to be about 1.5 times larger than that of the B form, and the cause of this difference is discussed. Interestingly, when the power of the excitation laser is increased, another type of TG signal is observed over a much longer time range. This TG signal is due to aggregate formation; the signal is attributed to the intensity grating produced by probe light scattering due to the aggregates. The kinetics of formation are examined on the basis of a diffusion-controlled reaction model.

2. Experimental details

The TG experimental set-up was similar to that reported elsewhere [14–22]. Briefly, the third harmonics of an Nd:YAG laser (Spectra Physics DC-11; $\lambda = 355$ nm) was used as excitation light. An He–Ne laser ($\lambda = 633$ nm) or Ar ion laser (Uniphase 2213) was used as the probe beam. The TG signal was detected by a photomultiplier (Hamamatsu R928) and the temporal profile was averaged by a digital oscilloscope (Tektronix 2430A). These data were transferred to a microcomputer for further analysis. The repetition rate of the excitation beam was about 2 Hz. When the dynamics of the aggregation process were monitored, a flowing sample was used to prevent large aggregates from remaining in the illuminated region. The fringe spacing (Λ) was determined from the decay rate of the thermal grating signal in a methyl red–benzene solution [16]. The TG experiment was performed at room temperature and the power of the pump beam was approximately 2 μJ per pulse for the observation of the diffusion process.

The spin echo method was used for the measurement of the self-diffusion constant of 8-nitroBIPS by an NMR (JEOL JNM-EX270, wide-bore type) spectrometer. The sample was contained in a 5 mm sample tube. A homospoil coil of the spectrometer was used to generate the magnetic field gradient (G) pulses. The spin echo signal was analysed by the relation [23]

$$I_{NMR} \propto \exp[-\gamma^2 G^2 \delta^2 D(\Delta - \delta/3)]$$

where γ is the magnetogyric ratio of the proton, δ is the gradient duration and Δ is the interval between the r.f. and gradient pulses. The parameters employed to determine D in this equation were calibrated using the D value of water ($D = 2.54 \times 10^{-9}$ m^2 s^{-1} at 30 °C) under the same experimental conditions.

8-nitroBIPS (Eastman Kodak) was used as received. Ethanol and cyclohexane (spectrograde from Nacalai Tesque) were used without further purification. The concentration of the sample was 0.5 mM for the observation of the monomer diffusion process.

3. Results and discussion

3.1. Diffusion processes of spiropyran monomers

After UV irradiation of the spiropyran A form, it is converted to the coloured B form (Scheme 1) [1]. At the same time, the excess energy from various relaxation processes is released to the matrix as heat. Therefore if the solution is irradiated by spatially sinusoidally modulated light, the same modulations of temperature and concentration of the created B form, as well as the antiphase modulation of the A form by depletion, are created in the solution. Since the refractive index and absorbance are functions of the temperature and concentration of these species, these modulations act as the (trarsient) grating which can be monitored by another probe beam (the TG signal). The time profile of the TG signal from such a photoinduced reversible chemical reaction system has been analysed previously. The intensity of the TG signal ($I_{TG}(t)$) is given by [24]

$$I_{TG}(t) = \alpha[\delta n(t)]^2 + \beta[\delta k(t)]^2 \quad (1)$$

where δn and δk are the peak to null differences of the refractive index and absorbance respectively. The temporal profiles of the $\delta n(t)$ and $\delta k(t)$ terms can be obtained by solving the diffusion equations and are given by [16]

$$\delta n(t) = \delta n_{th}^0 \exp(-D_{th} q^2 t) + \delta n_1^0 \exp(-D_A q^2 t) + \delta n_2^0 \exp[-(D_B q^2 + k_{BA})t]$$

$$\delta k(t) = \delta k_1^0 \exp(-D_A q^2 t) + \delta k_2^0 \exp[-(D_B q^2 + k_{BA})t]$$

and

$$\delta n_1 = -[\Delta b]\delta n_A \frac{D_B q^2 - D_A q^2}{D_B q^2 - D_A q^2 + k_{BA}}$$

$$\delta n_2 = [\Delta b]\left(\delta n_B - \delta n_A \frac{k_{BA}}{D_B q^2 - D_A q^2 + k_{BA}}\right)$$

$$\delta k_1 = -[\Delta b]\delta k_A \frac{D_B q^2 - D_A q^2}{D_B q^2 - D_A q^2 + k_{BA}}$$

$$\delta k_2 = [\Delta b]\left(\delta k_B - \delta k_A \frac{k_{BA}}{D_B q^2 - D_A q^2 + k_{BA}}\right)$$

where k_{BA} is the rate constant of the back chemical reaction process from the B form to the A form. The subscripts th, B and A denote thermal and the B and A forms respectively.

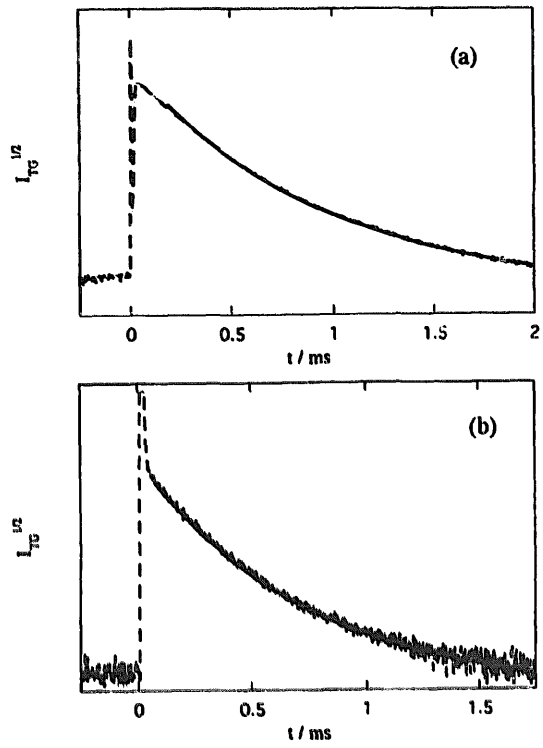

Fig. 1. Typical time profile of the TG signal after photoexcitation of 8-nitroBIPS in ethanol probed at 633 nm (a) and 458 nm (b) (broken lines). The signals in the fast time region originate from the thermal grating at both wavelengths. The slower part is due to the species grating. The full lines are the best-fit curves to Eq. 2 in (a) and Eq. 3 in (b).

$[\Delta b]$ is the concentration change of the B form by photoexcitation and q is the magnitude of the wavevector of the grating.

The observed TG signal after photoexcitation of 8-nitroBIPS in an ethanol solution probed by an He–Ne laser is shown in Fig. 1(a). The initial spike-like TG signal is due to the thermal grating, which decays with a time constant of thermal conduction between the fringes ($D_{th}q^2$). After the signal reaches the baseline, it rises to another peak and then decays again. This decay curve is well expressed by a single-exponential function as shown in Fig. 1(a). The time constant of the decay is about 2–3 orders of magnitude slower than the thermal diffusion time, which indicates that the decay represents the species diffusion between the grating fringes (the species grating).

The chemical species giving rise to this species grating can be easily identified from the absorption spectra of the A and B species. All of the absorption bands of the A species are located at wavelengths shorter than 400 nm, whereas a strong absorption band is observed at approximately 550 nm for the B species. The stronger absorption band near the probe wavelength may be the origin of the strong grating signal. Since there is a dip between the thermal grating signal and the species grating signal, the species grating should consist of a phase grating with a positive sign. Therefore I_{TG} of Eq. (1) can be reduced to

$$I_{TG}^{1/2}(t) = \alpha^{1/2}\delta n_2^0 \exp[-(D_B q^2 + k_{BA})t] \quad (2)$$

In Fig. 2(a), the decay rate constant of the species grating signal (k) is plotted against q^2. The plot gives a straight line with a small intercept, which indicates that the lifetime of the B species in ethanol is sufficiently longer than the diffusion time between the fringes. Indeed, the lifetime of the B form is very long compared with the time scale of this TG measurement in ethanol ($Dq^2 \gg k_{BA} \sim 10^{-4}\ s^{-1}$) [25]. The diffusion constant of the B species determined from the slope of Fig. 2(a) is given in Table 1.

The negligible contribution of the A form to the species grating signal is due to the fact that the absorption band of the A form is far from the He–Ne laser wavelength. We may be able to use a probe light with a shorter wavelength to investigate D of the A form. Fig. 1(b) shows the TG signal probed at 458 nm. At this wavelength, the absorption by the A and B forms is very weak, but the wavelength is still close enough to the absorption bands to give rise to a strong phase grating signal. Under this condition, the temporal profile of the species grating signal is expected to be expressed by

$$I_{TG}^{1/2}(t) = \alpha^{1/2}[-\delta n_1^0 \exp(-D_A q^2 t) + \delta n_2^0 \exp(-D_B q^2 t)] \quad (3)$$

where δn_1^0 and δn_2^0 should be positive and negative respectively. Indeed, the observed signal can be fitted well using a bi-exponential function. During the least-squares fitting of the curve, we fixed one decay rate constant $D_B q^2$, which was

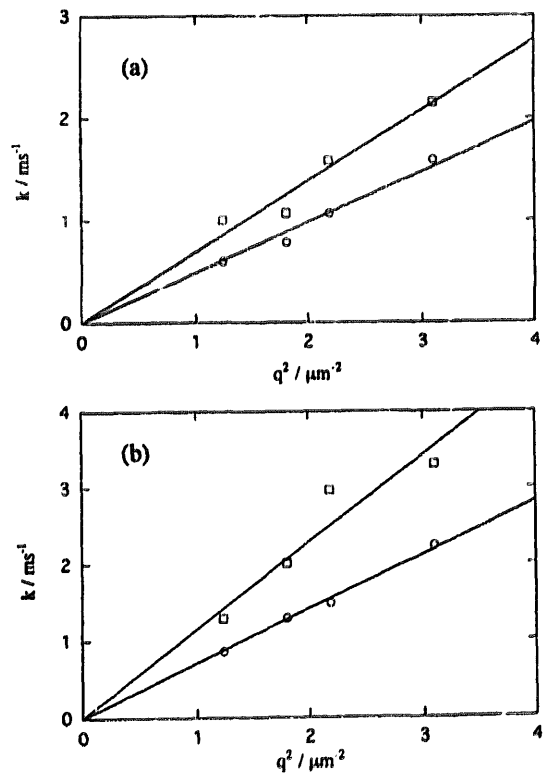

Fig. 2. Plot of the decay rate constants (k) of the TG signal against the square of the wavevector of the grating (q^2) in ethanol (a) and cyclohexane (b). Squares denote the decay rates of the TG signal due to the A form probed at 458 nm and circles denote the decay rates of the TG signal due to the B form probed at 633 nm.

Table 1
Diffusion coefficients (D) of the colourless (A) and coloured (B) forms of 8-nitroBIPS, and calculated values by the Stokes–Einstein (SE) relation

Solvent	D_A (10^{-9} m^2 s^{-1})	D_B (10^{-9} m^2 s^{-1})	D_{SE}^a (10^{-9} m^2 s^{-1})	D_{SE}^b (10^{-9} m^2 s^{-1})
Ethanol	0.69	0.49	0.747	0.498
Cyclohexane	1.1	0.71	0.900	0.600

[a]Slipping boundary condition.
[b]Sticking boundary condition.

determined previously using the He–Ne laser, because the difference between the two decay rate constants is too small to be determined simultaneously by the fitting.

Slightly different features are observed in the TG signal of 8-nitroBIPS in cyclohexane. The TG signal probed with the He–Ne laser is shown in Fig. 3(a). The signal seems to lack a thermal grating. This is not due to the weak thermal grating signal, but to the very strong species grating. The strong species grating can be explained by the strong absorption of the B form at the He–Ne laser wavelength. (The absorption band of the B form shifts to the red region in non-polar solvents; the wavelength of the peak is approximately 600 nm compared with approximately 550 nm in ethanol.) The dominant contribution of the δk term can be verified by a very weak interference dip between the thermal grating and the species grating.

The decay curve can be expressed by a single-exponential function, and the rate constant should represent the diffusion time of the B species. The decay rate constant (k) is proportional to q^2 as shown in Fig. 2(b). Again the intercept is very

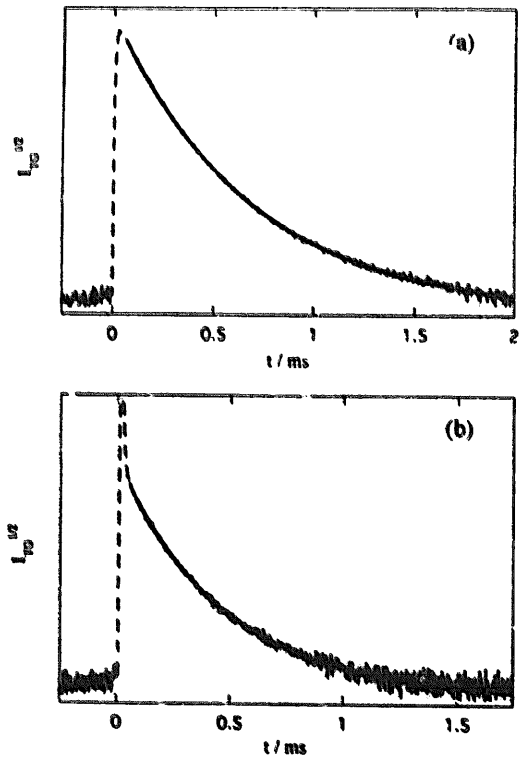

Fig. 3. Time profile of the TG signal of 8-nitroBIPS in cyclohexane probed at 633 nm (a) and 458 nm (b) (broken lines). The full lines are the best-fit curves to Eq. 2 in (a) and Eq. 3 in (b).

small, which is consistent with the rather slow back reaction from the B species to the A species (approximately 200 ms in cyclohexane). D of the A species in cyclohexane can be determined by the same method as in ethanol by using a shorter wavelength for the probe. Fig. 3(b) shows the TG signal observed at a probe wavelength of 458 nm. This signal is similar to that in ethanol, and the temporal profile can be represented by a bi-exponential function. One of the time constants is D_Bq^2 and the other should be D_Aq^2. The rate constant plotted against q^2 shows a linear relationship and D_A can be obtained from the slope (Table 1). To support the accuracy of this experiment, D_A in cyclohexane-d_{12} was measured by the NMR spin echo method. The value is $D_A = 0.96 \times 10^{-9}$ m^2 s^{-1}, which is close to D_A from the TG experiment in cyclohexane solution. The diffusion constant of the B species is found to be about 1.4 times smaller than that of the A species. Since all the rate constants in this section show no pump laser power dependence, there is no influence of aggregate formation.

Next, we examine the origin of the difference between D_A and D_B. Frequently, the diffusion constant in solution is calculated using the Stokes–Einstein (SE) equation

$$D = k_BT/a\pi r\eta \quad (4)$$

where k_B is the Boltzmann constant, r is the radius of the diffusing molecule, η is the viscosity of the solution and $a = 4$ in the slipping boundary condition and $a = 6$ in the sticking boundary condition. If we calculate the van der Waals' volume of the molecule by the group increment method [26] and r is defined by the radius of a sphere which has the same volume as the van der Waals' volume, the radius of the A form is not very different from that of the B form (the radii of the A form (r_A) and B form (r_B) are 0.407 nm and 0.410 nm respectively). This difference cannot explain the observed ratio of D_A/D_B as long as the boundary condition remains unchanged between these two species.

Another factor which should be taken into consideration is the change in molecular structure from the A form to the B form. While the A form is close to a spherical shape, various planar lengthened shapes are suggested for the B form. The friction of diffusion, which is defined by $f = kT/D$, of an ellipsoidal molecule can be roughly estimated by the equation [27]

$$\frac{f}{f_0} = \frac{2(1-b^2/a^2)^{1/2}}{(b/a)^{2/3}\ln\{[1+(1-b^2/a^2)^{1/2}]/[1-(1-b^2/a^2)^{1/2}]\}} \quad (5)$$

where f_0 is the friction of a sphere, f is the friction of an ellipsoid, a is the radius of the major axis and b is the radius of the minor axis. In this case, we assume that the A form is spherical and that the B form is a prolate having an axial ratio $b/a = 0.434$, which is estimated from the molecular structure and the van der Waals' radii. With this assumption, the ratio of the friction of the B form to that of the A form is calculated as $f_B/f_A = 1.07$. Therefore the change in molecular structure from the A form to the B form cannot explain the large reduction in D. We believe that the large electric dipole moment of the B form is the origin of the reduction. When the diffusing molecule has an electric dipole, the dipole will interact with the surrounding solvent molecules increasing the friction during diffusion.

It is interesting to note that D_A is close to D_{SE} with the slipping boundary condition, whereas D_B is close to D_{SE} with the sticking boundary condition. The effect of the charge on D has been investigated for many systems. For example, Evans et al. [28,29] have investigated the D values of electrically neutral and charged molecules with spherical shapes and have found that D is strongly dependent on whether or not the molecules are charged. Moreover, it is well known that the rotational diffusion constants of charged dye molecules are close to those calculated on the basis of the Debye–Stokes–Einstein relation with the sticking boundary condition, while those of neutral molecules are close to those calculated with the slipping boundary condition [30]. However, these observations depend on the molecular size. The difference in D between charged and neutral molecules is very large for small molecules, but decreases with increasing size. The results of Evans et al. [28,29] show that, for a size comparable with 8-nitroBIPS, the D values of uncharged and charged molecules are close to D_{SE} with the slipping and sticking boundary conditions respectively . Our results ($D_A \sim D_{SE}$ (slip) and $D_B \sim D_{SE}$ (stick)) are consistent with the results of Evans et al. [28,29].

In cyclohexane, the ratio D_A/D_B is 1.5, and D_A is close to D_{SE} with the slipping boundary condition and D_B is close to D_{SE} with the sticking boundary condition. This is similar to the observations in ethanol solution. Therefore the effect of the electric dipole of the B form also exists in non-polar solvents in this system.

3.2. Formation process of the aggregates

When the pump laser power is increased to approximately 20 μJ per pulse for 8-nitroBIPS–cyclohexane (2.5 mM), another new signal appears over a much longer time scale than the species grating signal (Fig. 4(a)). This new signal disappears when the probe beam or the pump beams are blocked before the sample. Furthermore, the signal disappears when the pinhole for detection is moved from the phase matching direction. On this basis, we attribute this feature to another TG signal and not to luminescence or light scattering. The temporal profile and intensity of this signal are sensitive to the excitation laser power and the concentration of the sample. This type of TG signal is not observed in ethanol solution.

The temporal profile of the signal can be approximately expressed by a bi-exponential function

$$I_{TG}^{1/2}(t) = a_s \exp(-k_s t) + a_f \exp(-k_f t) \quad (6)$$

where $a_s a_f < 0$ and $k_f > k_s$. The q^2 dependence of k_s and k_f was measured and is shown in Fig. 5. k_s and k_f are almost proportional to q^2. This proportional relation indicates that both the rise and decay rates are governed by the diffusion process in the solution. From the slope of the q^2 vs. k plot, diffusion constants for the rise (D_f) and decay (D_s) can be determined: $D_f = 3.6 \times 10^{-10}$ m^2 s^{-1} and $D_s = 3.2 \times 10^{-11}$ m^2 s^{-1}. If we calculate the size of the diffusing species from D_s and D_f based on the Stokes–Einstein equation with the sticking boundary condition, the r values for the rise (r_f) and decay (r_s) are 0.81 nm and 9.1 nm respectively. These radii correspond to about 7 molecules and about 11 000 molecules of the B form.

In non-polar solvents, microcrystals of nitroBIPS are produced by UV irradiation [4,5,7]. The microcrystals are composed of many AB and A_nB ($n = 2, 3$) moieties; the sizes of the microcrystals are 10–40 nm, i.e. close to the radii estimated above. Indeed, under the condition in which the new TG signal is observed, light scattering of the probe beam is also observed from the TG region by the naked eye, which indicates that aggregates are induced by the excitation light.

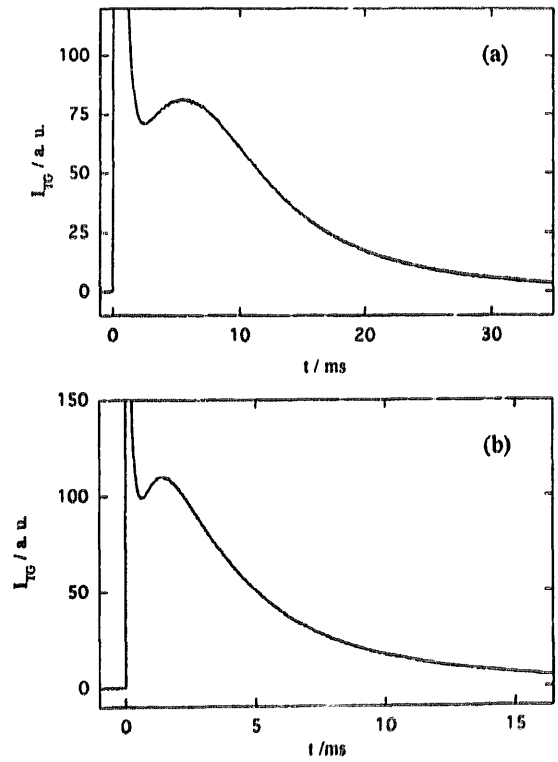

Fig. 4. Observed TG signal at strong pump laser power. The initial part of the signal is mainly due to the species grating of the B form. The slower part is called the aggregate grating signal. The concentration of the sample is 2.5 mM and the square of the wavevector of the grating is $q^2 = 1.59$ μm^{-2} (a) and $q^2 = 4.27$ μm^{-2} (b).

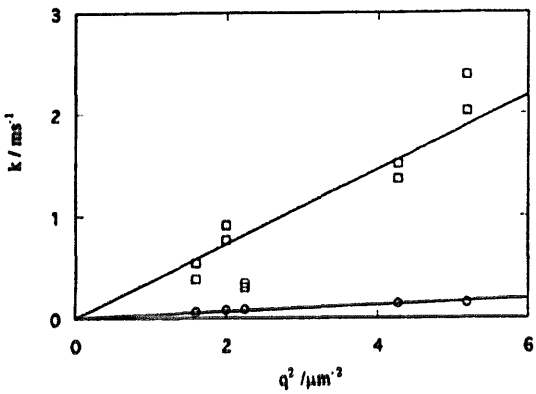

Fig. 5. Plot of the decay or rise rate constant (k) vs. the square of the wavevector of the grating (q^2). The squares denote the rise rate constants (k_r) and the circles denote the decay rate constants (k_s).

Considering the reported aggregate formation in non-polar solvents and the calculated size of the diffusing species, we attribute the new TG signal on the slow time scale to the microcrystals. It is interesting to note that the TG signal of the aggregates rises after the species grating signal of the monomers has disappeared by diffusion. It is curious that the aggregates form a grating after the spatial distribution of the monomers becomes uniform in the solution.

There are two necessary conditions for observing this phenomenon: the probe diffraction efficiency of the aggregate must be larger than that of the monomer and the aggregate should form a spatial grating in the solution. First, let us consider the first condition. Generally, the TG signal appears by spatial modulation of the refractive index or absorption of the samples as shown in Eq. (1). The higher efficiency of diffraction of the aggregates may indicate that the refractive index and absorption of the aggregates are much larger than those of the monomer. If the aggregates are microcrystals, which are reported as J-aggregates [5,7], the optical properties of the aggregates can be described by exciton theory [31]. According to exciton theory, the transition dipole moment of the aggregates will be a vector sum of that of the monomers in the unit cell. Therefore, although the absorption coefficient of each microcrystal will increase as the crystal grows, the total absorption coefficient in the total system should remain nearly constant. Moreover, the peak of the absorption band of the microcrystal shifts to the red of the wavelength of the He–Ne laser with increasing aggregation number [12,13]. Therefore it is rather unrealistic to believe that the absorption and refractive index of the aggregates are much larger than those of the monomer.

Since the ordinary mechanism of the TG signal cannot explain the observed behaviour, we believe that light scattering may introduce a modulation of the optical properties. According to the theory of light scattering by a small particle, the scattering efficiency is proportional to the square of the volume of the scattering obstacle [32]. Therefore if the aggregate becomes larger, the efficiency of light scattering increases and a stronger TG signal is expected from the aggregate than from the monomer.

The other necessary condition is related to how the aggregates form in solution. There are two possible mechanisms which can explain the formation of the aggregate grating after the species grating of the monomer has disappeared. First, the core of the microcrystal may be adhesively attached to the surface of the sample cell at a short initial time after photoexcitation and, gradually, AB and A_nB will be accumulated on the core to yield the microcrystal. This mechanism seems to be reasonable since microcrystals are easily accumulated on the cell surface.

In order to examine this mechanism, we carried out a similar TG experiment but without the cell surface. For this purpose, the sample solution was contained in a bottle without a cover and with a flat, clean and transparent bottom. The pump and probe beams for the TG experiment were passed to the sample via the air–sample surface; the crossing area for the three beams was limited to near the surface. The TG signal was detected from the bottom. Even under this window-free condition, we observe the rise in the aggregate grating signal after the decay of the species grating. Therefore we must conclude that the window of the cell is not essential for the slow rise of the aggregate grating. In order to explain the rise, we assume that small (larger than the monomer) cores are created in the solution by the sinusoidally modulated concentration of the B form. If the cores are sufficiently larger than the monomer, the diffusion of the cores is negligible during the diffusion process of the monomer between the fringes. After the modulation due to the monomer is smeared out, the monomers are gradually gathered on the cores to produce the aggregates. The combination of the slow growth of the aggregates to form a spatially modulated pattern and the large efficiency of light scattering will lead to a slow rise in the TG signal due to the aggregate grating.

We also investigated the pump laser power dependence and the concentration dependence of the aggregate grating signal. When the laser power is increased, k_s in Eq. (6) decreases and k_f increases (i.e. the aggregate grating signal rises rapidly and decays slowly). When the concentration of the solution is increased, k_s decreases and k_f increases. These observations can be explained consistently with the above proposed mechanism as follows. When the power is strong or the concentration is large, larger aggregates are produced rapidly and large aggregates diffuse slowly.

We tried to reproduce the temporal profile of the signal based on this mechanism as follows. We assumed that, 1 ms after excitation, there are only two sorts of aggregates: small and large. Small aggregates (Y) contain about seven monomers and are spread over all the fringe spacings uniformly. The size of Y is estimated from the size calculated by D_f. Large aggregates (X) (size ten times larger than Y) also exist in the bright region of the optical grating. The distribution of X gives a sinusoidal pattern; the initial concentrations of these aggregates are given by

$$[X] = [X]_0(1 - \cos qx) \quad (7a)$$

$$[Y] = [Y]_0 \quad (7b)$$

As time goes by, the following aggregation reaction occurs

$$X+Y \rightarrow XY$$

$$XY+Y \rightarrow XY_2$$

$$XY_{n-1}+Y \rightarrow XY_n$$

We assume that this aggregation process is terminated at XY_n ($n=400$), i.e. XY_{n+1}, XY_{n+2},... are not produced. If the aggregation process does not stop, the intensity of the calculated aggregate grating signal increases monotonically and does not reach a maximum in a reasonable time range. This assumption is consistent with the fact that the previously observed microcrystal had a similar size to XY_n ($n \approx 400$) [5]. This termination is also consistent with the fact that we could not observe macroscopic crystals visually under these experimental conditions. The deaggregation process is not considered in this calculation, because it is reported to be very slow (10^{-1}–10^{-2} s^{-1}) compared with the formation process [11]. If the aggregation processes are diffusion controlled, the formation rate constant for the aggregate XY_k is given by [33]

$$k_k = 4\pi P(D_{k-1}+D_Y)(r_{k-1}+r_Y)N_A \quad (8)$$

where P is the reaction probability per collision, D_{k-1} and D_Y are the diffusion coefficients of XY_{k-1} and Y respectively, r_{k-1} and r_Y are the radii of XY_{k-1} and Y respectively and N_A is Avogadro's number. The factor P in Eq. (8) represents the fact that aggregation occurs through the nitro group [9,11] and there should be a favourable direction for aggregation. The radius r is estimated from the volume of the aggregate and the radius of the B form. D is calculated by the Stokes–Einstein relation using the D value of the B form and r_B/r as follows

$$r_k = \sqrt[3]{r_X^3 + k r_B^3} \quad (9)$$

$$D_k = D_B r_B / r_k \quad (10)$$

where r_X is the radius of X. The time evolutions of the concentrations of these aggregates are given by

$$\frac{\partial[XY_k]}{\partial t} = D_k \frac{\partial^2}{\partial x^2}[XY_k] + k_k[Y][XY_{k-1}] - k_{k+1}[Y][XY_k] \quad (11)$$

$$\frac{\partial[Y]}{\partial t} = D_Y \frac{\partial^2}{\partial x^2}[Y] - k_1[Y][X] - k_2[Y][XY] - \cdots - k_n[Y][XY_{n-1}] \quad (12)$$

where $k = 1, 2, ..., n-1$. The first term on the right-hand side of Eq. (11) is the diffusion term of the aggregate XY_k. The second term represents the formation reaction and the third term an extinction reaction. When $k=0$ and n, there should be no third term and second term respectively because of our assumption. Thus aggregates larger than $n+1$ are not produced. To calculate the time evolution of the distribution of each aggregate in a fringe spacing, we divide one fringe spacing into 128 parts at regular intervals and, at each point, we calculate numerically the time evolution using finite differential equations of Eqs. (11) and (12).

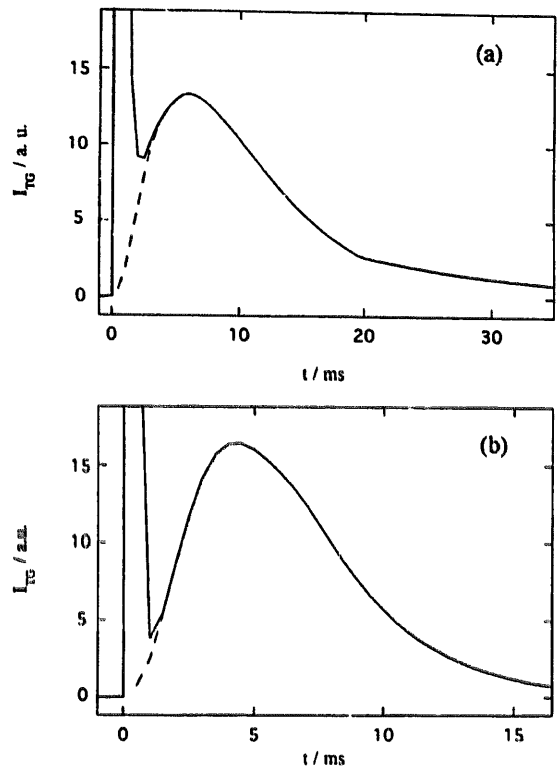

Fig. 6. Calculated TG signals based on the aggregate formation model given in Section 3.2: (a) $q^2 = 1.59$ μm^{-2}; (b) $q^2 = 4.27$ μm^{-2}. The parameters for the calculations are listed in Table 2. The broken line is the pure aggregate grating signal and the full line is the total TG signal (sum of the aggregate grating signal and the species grating signal due to the monomer of the B form).

After the spatial distributions of these aggregates have been obtained, the TG signal intensity from each component is calculated in the following manner. First the Fourier component of each distribution is calculated at each time. Since the origin of the aggregate grating signal is the scattered light, and the diffraction efficiency by Rayleigh scattering is considered to be proportional to the square of the volume of the scattering obstacle [31], the size-dependent diffraction efficiency should be taken into account. For this purpose, the square of the volume of each aggregate is multiplied by the Fourier component at q. These values are summed for $[XY_k]$ ($k=0$–n) to obtain the aggregate grating signal intensity.

First, we calculate the aggregate grating signal under the same conditions as those of Fig. 4(a). The initial concentration of Y ($[Y]_0$) is calculated using the assumption that all monomers convert to Y. The initial concentration of X ($[X]_0$) is set to $[Y]_0/n$. The best-fit calculated signal is shown in Fig. 6(a). The parameters used are listed in Table 2. The agreement between the calculated and observed TG signals is satisfactory. The calculated profile is sensitive to the parameters. For example, if P is larger than the value given in Table 2, the rise of the aggregate grating signal becomes more rapid, indicating a more efficient creation of the aggre-

Table 2
Parameters used for the calculation of the aggregate grating signal Fig. 6

n	400
$[X]_0$	9×10^{-7} M
$[Y]_0$	3.6×10^{-4} M
P	0.03
r_B	0.410 nm
D_B	0.71×10^{-9} m^2 s^{-1}

gate. When the initial concentration is set to a lower value, the calculated aggregate grating signal shows a slower rise and decay. This is not consistent with the results observed on reducing the sample concentration. In order to fit the grating signal at a lower concentration, the aggregation numbers of X and Y, as well as XY_n, must be smaller. In other words, the aggregation numbers depend on the sample concentration and the laser power. This dependence seems to be reasonable because small aggregates should be formed at low concentrations.

Next, when only q^2 is changed in the calculation from 1.59 to 4.27 μm^{-2}, keeping the other parameters the same as in Table 2, we obtain a calculated signal as shown in Fig. 6(b). The calculated signal shows a faster rise and decay of the aggregate grating, which is consistent with the observations. However, quantitatively, the q^2 dependence of the rate is not as significant as that observed. One of the main reasons for the discrepancy is probably that our model is too simple to describe real aggregate formation. For example, various aggregation processes should occur in the real system (e.g. $X+X\rightarrow X_2$ etc.), which are not considered in our model. However, it is important to stress that the TG signal calculated on the basis of our model reproduces the essential features observed experimentally. From this calculation, the following observations can be made: (1) a small aggregate Y, consisting of about seven monomers, is created as well as a large aggregate X (approximately 100 monomers) within a few hundred microseconds after photoexcitation; (2) the smaller aggregates Y accumulate on X to produce microcrystals; (3) the aggregate (microcrystal) of 8-nitroBIPS contains approximately 3000 monomers, depending on the experimental conditions (concentration, laser power); (4) the formation of the aggregates is a diffusion-limited process with a rather low reaction probability.

4. Conclusions

We have investigated the molecular dynamics after UV irradiation of a photochromic molecule, 8-nitroBIPS, in ethanol and cyclohexane by the time-resolved TG method. When the excitation laser power is weak, the thermal grating and species grating signals due to the colourless (A) and coloured (B) forms are observed. By analysing the grating signal probed at various wavelengths, the D values of the A and B forms can be determined. The D value of the neutral A form is about 1.5 times larger than that of the charge-separated B form, and the reduction of D of the B form is discussed in terms of the charge separation in the B form.

In cyclohexane, when the excitation laser power is increased, a new type of TG signal is observed over a much longer time range than the thermal and species grating signals. We attribute this new signal to probe beam diffraction by a grating made up of aggregates of A and B forms (aggregate grating). The origin of the sinusoidal modulation of the optical property is attributed to Rayleigh light scattering by the aggregates. The observed temporal profile can be reproduced by a calculation based on a diffusion-controlled reaction model for the production of the aggregates. This signal may be used to elucidate the dynamics of aggregate formation, which is usually very difficult by other spectroscopic techniques.

Acknowledgements

We thank Professor M. Nakahara and Mr. H. Saito (Kyoto University) for measurement of the diffusion coefficient of 8-nitroBIPS in cyclohexane-d_{12} by NMR.

References

[1] G.H. Brown (ed.), *Photochromism*, Wiley-Interscience, New York, 1971.
[2] V.A. Krongauz and A.A. Parshutkin, *Photochem. Photobiol.*, *15* (1972) 503.
[3] A.A. Parshutkin and V.A. Krongauz, *Mol. Photochem.*, *6* (1974) 437.
[4] V.A. Krongauz and E.S. Goldburt, *Nature*, *271* (1978) 43.
[5] V.A. Krongauz, S.N. Fishman and E.S. Goldburt, *J. Phys. Chem.*, *82* (1978) 2469.
[6] V.A. Krongauz and E.S. Goldburt, *Chem. Phys. Lett.*, *60* (1979) 251.
[7] V.A. Krongauz, *Isr. J. Chem.*, *18* (1979) 304.
[8] V. Krongauz, J. Kiwi and M. Grätzel, *J. Photochem.*, *13* (1980) 89.
[9] Y. Onai, K. Kasatani, M. Kobayashi, H. Shinohara and H. Sato, *Chem. Lett.*, (1990) 1809.
[10] H. Sato, H. Shinohara, M. Kobayashi and T. Kiyoyama, *Chem. Lett.*, (1991) 1205.
[11] Y. Onai, M. Mamiya, T. Kiyoyama, K. Okuwa, M. Kobayashi, H. Shinohara and H. Sato, *J. Phys. Chem.*, *97* (1993) 9499.
[12] Y. Kalisky and D.J. Williams, *Chem. Phys. Lett.*, *86* (1982) 100.
[13] Y. Kalisky and D.J. Williams, *Macromolecules*, *17* (1984) 292.
[14] M. Terazima and N. Hirota, *J. Chem. Phys.*, *95* (1991) 6490.
[15] M. Terazima and N. Hirota, *J. Chem. Phys.*, *98* (1993) 6257.
[16] M. Terazima, K. Okamoto and N. Hirota, *J. Phys. Chem.*, *97* (1993) 5188.
[17] M. Terazima, K. Okamoto and N. Hirota, *J. Phys. Chem.*, *97* (1993) 13 387.
[18] M. Terazima, K. Okamoto and N. Hirota, *J. Chem. Phys.*, *98* (1993) 6257.
[19] M. Terazima, *Chem. Phys. Lett.*, *218* (1994) 574.
[20] K. Okamoto, M. Terazima and N. Hirota, *J. Chem. Phys.*, *103* (1995) 10 445.
[21] K. Ohta, M. Terazima and N. Hirota, *Bull. Chem. Soc. Jpn.*, *68* (1995) 2809.
[22] M. Terazima, T. Okazaki and N. Hirota, *J. Photochem. Photobiol. A. Chem.*, *92* (1995) 7.
[23] P. Stilbs, *Prog. Nucl. Magn. Reson. Spectrosc.*, *19* (1987) 1.

[24] H.J. Eichler, P. Günter and D.W. Pohl, *Laser-Induced Dynamic Gratings*, Springer, Berlin, 1986.
[25] J.B. Flannery, Jr., *J. Am. Chem. Soc.*, *90* (1968) 5660.
[26] J.T. Edward, *J. Chem. Educ.*, *47* (1970) 261.
[27] R.O. Herzog, R. Illig and H. Kuder, *Z. Phys. Chem.*, *167A* (1933) 329.
[28] D.F. Evans, C. Chan and B.C. Lamartine, *J. Am. Chem. Soc.*, *99* (1977) 6492.
[29] D.F. Evans, T. Tominaga, J.B. Hubbard and P.G. Wolynes, *J. Phys. Chem.*, *83* (1979) 2669.
[30] G.R. Fleming, *Chemical Applications of Ultrafast Spectroscopy*, Oxford University Press, Oxford, 1986.
[31] V. Czikklely, H.D. Forsterling and H. Kuhn, *Chem. Phys. Lett.*, *6* (1979) 207.
[32] C.F. Bohren and D.R. Huffman, *Absorption and Scattering of Light by Small Particles*, Wiley, New York, 1983.
[33] A.H. Alwattar, M.D. Lumb and J.B. Birks, in J.B. Birks (ed.), *Organic Molecular Photophysics*, Vol. 1, Wiley, London, 1973.